2009

Computational and experimental investigation of the flow structure and vortex dynamics in the wake of a Formula 1 tire

John Axerio

Gianluca Iaccarino

Emin Issakhanian
Loyola Marymount University, emin.issakhanian@lmu.edu

Chris Elkins

John Eaton

Paper Number 09B-0082

Computational and Experimental Investigation of the Flow Structure and Vortex Dynamics in the Wake of a Formula 1 Tire

John Axerio, Gianluca Iaccarino
Center for Turbulence Research, Department of Mechanical Engineering, Stanford University, CA

Emin Issakhanian, Kin Lo, Chris Elkins, John Eaton
Department of Mechanical Engineering, Stanford University, CA

ABSTRACT

The flow field around a 60% scale stationary Formula 1 tire in contact with the ground in a closed wind tunnel is examined experimentally in order to validate the accuracy of different turbulence modeling techniques. The results of steady RANS and Large Eddy Simulation (LES) are compared with PIV data - performed within the same project. The far wake structure behind the wheel is dominated by two strong counter-rotating vortices. The locations of the vortex cores, extracted from the LES and PIV data as well as computed using different RANS models, show that the LES predictions are closet to the PIV vortex cores. All turbulence models are able to accurately predict the region of strong downward velociy between the vortex cores in the centerplane of the tire, but discrepancies arise when velocity profiles are compared close to the inboard and outboard edges of the tire, due to the sensitivity of the solution to the tire shoulder modeling. In the near wake region directly behind the contact patch of the tire, contour plots of inplane-velocity are compared for all three datasets. The LES simulation again matches well with the PIV data.

INTRODUCTION

An important motivation for modeling the flow around tires is due to their impact on the total drag of the car [1]. In addition, controlling the wake dynamics, increasing downforce, improving brake/engine cooling can all be achieved by knowing the exact details of wake structures. Wheel covers have become wide spread in Formula 1 for the aforementioned reasons. Currently, teams have time constraints that limit the use of high fidelity simulation tools such as LES. They are typically limited to engineering methods (such as RANS) that have been proven to perform poorly in regions of large separation [2] and strong unsteadiness such as the region in the immediate wake of the tire.

This paper has two main objectives, and is the first of a set of papers that would like to quantify the uncertainty in the wake dynamics of wheels due to uncertain input parameters. The first purpose is to compare RANS and LES data side by side for near wake in-plane velocity measurements. The second purpose is to quantify the effect of using different turbulence models on determining vortex core locations behind the tire. It is important to try to identify the limitations of certain turbulence models, and which parameters have the greatest effect on the solution. Non-linearity and anisotropic effects can greatly reduce the accuracy of typical turbulence models. As a result, the deficiencies of modeling more of the turbulence (RANS compared to LES) should be apparent in regions of large separation as is shown in this paper.

There is a significant amount of information in the literature concerning both stationary and rotating tires. Fackrell and Harvey [3] have performed experimental measurements of the aerodynamic force and pressure distribution around the tire. Since then, many other papers have presented detailed work both experimentally and computationally on the pressure distribution around the tire, but since we are concerned with wake dynamics these will not be discussed here. Nigbur [4] used a hot-wire anemometer (HWA) to measure the wake velocities of a 50% scale Formula 1 tire extracting mean profiles as well as RMS fluctuations. He showed that the wake structure was strongly asymemetric, possibly due to regions of high turbulent intensity in the wake of the strut. The HWA he used was insensitive to the direction of streamwise velocity, therefore he was not able to show regions of reversed flow. Wäschle [5] also made laser Doppler anemometry measurements in the wake of a

stationary and rotating Formula 1 tire and compared the data to different numerical codes. He was able to show reversed flow regions in the near wake, but the two main counter rotating vortices near the ground were poorly captured due to low resolution.

Computationally, RANS has been the most widely used method to compute the flow field around the tire. Recently, other approaches have become popular due to well known issues of RANS modeling. Wäschle [5] showed that improved predictions were possible using the Lattice-Boltzmann approach compared to RANS. McManus et al. [6] performed a computational study of both stationary and rotating wheels using the unsteady RANS (URANS) method and compared these to the Fackrell and Harvey geometry. They showed good agreement with the experiments, as well as giving a general schematic of the flow, including details of coherent structures that were not shown previously using RANS. To date, there have been no studies on tires performed using Large-Eddy Simulation (LES). A comparison of this method with common RANS approaches is the main contribution of this paper.

WHEEL MODEL

The tire assembly consists of a 60% scale model of a right front Formula 1 tire with wheel covers. The Reynolds number based on the wheel diameter and inlet velocity is 5.0e5. Unlike the experimental studies in the past of Knowles [7], as well as Saddington [8] the tire is completely deformable. The tire is held in place in the tunnel test section by a strut shrouded by a symmetric airfoil. The tire is then deformed by applying a load to the strut outside of the wind tunnel test section, deflecting the tire downwards to operating conditions representative of a Formula 1 race. It is essential to preserve the exact shape of the contact patch and tire sidewall profile because it has been proven in the past [9] that correct modeling of the tire shoulder is imperative to accurately predict the flow field. Different camber angles are tested (2.5° and 3.25°) to verify the sensitivity of the wake to wheel camber.

The wheel model as tested in this study both experimentally and computationally is shown in Figure 1. The wheel model is an exact replica of a Formula 1 wheel with covers on the inboard and outboard sides of the wheel hub that completely impede any flow from moving through the tire.

EXPERIMENTAL SETUP - PIV experiments are conducted in a closed-circuit wind tunnel with a 3.7m long, 0.61m wide, and 0.91m high test section. The tests are run at 18.4m/s with freestream turbulent intensity less than 0.5%. PIV measurements are obtained by using a laser, CCD camera, synchronizer, and data collection software. A dual head pulsed Nd:YAG laser is used to illuminate planes that are seeded with a fog machine. Velocity measurements with spatial resolution of 1.5mm by 1.5mm are obtained in planes of constant X (downstream of the tire) and Y by averaging 600 PIV image pairs taken at 2.5 Hz at different camera and laser sheet locations.

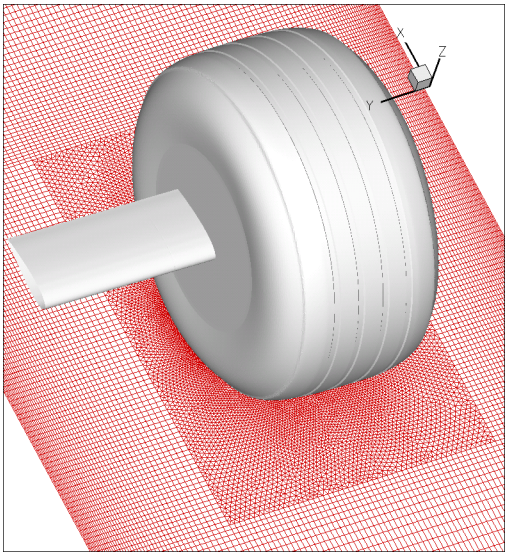

Figure 1: Computational model of the wheel showing the mesh details near the ground plane of the wind tunnel

COMPUTATIONAL GRID - A CAD model of the full wheel assembly is used as a starting point to remove unwanted parts and create an exact model of the experimental wheel. The wind tunnel walls, strut, and wheel covers are then added within the CAD environment and exported into a meshing program. It should be noted that in order to preserve cell quality near the bottom of the tire a very thin platform (2mm) is extruded from the outline of the contact patch. This technique enables the continuation of the prism layers which are needed to accurately model the boundary layer (Figure 2).

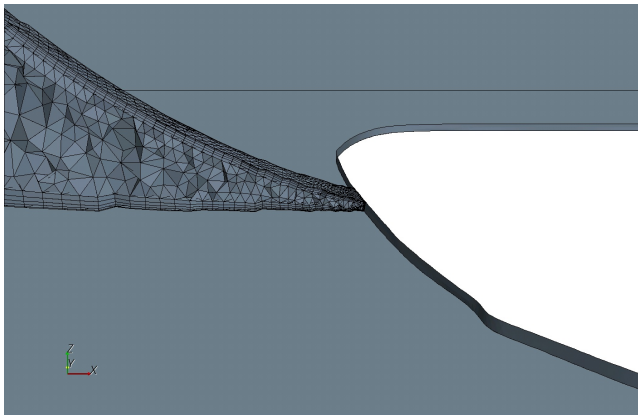

Figure 2: Mesh slice detail near the interface of the tire and ground showing the unstructured tetrahedral grid with 5 prism layers

Different meshing strategies were tested to determine the effect of the grid on the convergence of iterative calculations. In the end, a hybrid approach is adopted which consists of tetrahedrals in the immediate vicinity of the tire, and hexahedrals everywhere else. Creating a fully structured grid with such complex geometry is prohibitive. Five prism layers are used on all walls in the tetrahedral volumes to capture as much of the near wall viscous layers as possible. Two meshes, a coarse (7 million cells) and fine (40 million cells) mesh were generated and used in this study.

COMPUTATIONAL METHOD

LES SOLVER - LES simulations are performed for both the fine and coarse cell meshes using the Center for Turbulent Research fully unstructured code called CDP [10]. It uses a Smagorinsky type model for the subgrid scale turbulent fluxes. The flow field is initialized with the inlet velocity, and the initial time step is set at 1e-6s. All walls are set as stationary no slip surfaces, and the inlet velocity is 18.4 m/s. After an initial startup period a constant CFL number of 1.8 is used. Time averaging is initiated after 4 flow-through times.

Convergence of the mean velocity statistics for the LES computation is achieved when the statistics of higher order moments are no longer changing in time. Typically, low order moments (mean, variance) converge faster than higher orders, and this was the case for both the fine and coarse LES simulations. The higher order statistics are still not fully converged with the fine mesh simulation, but a good qualitative comparison of mean values with RANS is possible. The computational time required for the coarse mesh was about 25 days using 128 processors. In that time about 2 seconds (real time) of data was used for averaging (which accounts for approximately 90 flow-through times based on wheel diameter). The time required for the fine 40 million cell mesh was 60 days using 192 processors. About 0.7 seconds of data was used for averaging which accounts for approximately 30 flow-through times.

RANS SOLVER - Several RANS closures were used in this study, the k-ϵ model, k-ω model, Reynolds Stress model, and Spalart Allmaras model. Only the realizable k-ϵ model (RKE) results for the inplane-velocity are presented here because it has been shown in the past by Shih [11] that the RKE model performs fairly well in regions of large-scale separation. In addition, the high eddy viscosity typical of the RKE model is wake stabilizing. Bluff body flows are inherently unsteady; as a result, due to the vortex shedding, it is very difficult to converge the solution to steady-state, as was experienced by Basara [12]. When using the k-ω model for instance, the residuals do not fall to the same level as the RKE model. Instead, the two main counter-rotating vortices that dominate the wake (for x/D $>$ 1 downstream) oscillate slightly around a nominal position.

The discretization schemes of the RANS equations for momentum and turbulent quantities were initially set to first order and then switched to second order for all quantities including turbulent scalars. The solution was deemed to be converged when all residuals reduced by 5 order of magnitudes as well as the drag on the wheel not changing by more than 10 drag counts per iteration. This was not often possible with some RANS models due to the previously mentioned regular oscillations in the wake; this phenomenon was also experienced by Axon [13]. The computational resources needed for the coarse mesh was less than 1 day using 64 processors.

Boundary Conditions for RANS Solver - Since this simulation involves a stationary wheel, all walls are treated as no slip surfaces including the wind tunnel walls in the simulation. The boundary condition at the entrance of the wind tunnel is set as velocity inlet with the following turbulent inflow conditions:

$$k = \frac{3}{2} I^2 U^2 \tag{1}$$

$$\epsilon = \frac{k^2}{\nu Re_\tau} \tag{2}$$

Where I is the measured turbulent intensity of the wind tunnel, U is the mean velocity at the inlet of the wind tunnel, ν is the kinematic viscosity of air, ϵ is the dissipation, and Re_τ is the turbulent Reynolds number. It is quite important to specify the correct turbulent intensity at the inlet. Different turbulent intensities were tested to quantify the sensitivity of this parameter on the flow solution, and although there were minimal differences between 5% and 9% turbulent intensity, the results have shown a significant difference between 1% and 5% turbulent intensity.

The exit of the wind tunnel is set to a pressure outlet boundary condition. Initially an outflow boundary condition was used, but this condition did not allow the solution to converge to the specified tolerance.

RESULTS AND DISCUSSION OF WAKE FLOW STRUCTURES

The near wake of the tire (for x/D $>$ 0.8 downstream of the tire) is dominated by two large counter-rotating vortices. The vortical structures in the wake can be shown by using the λ_2 technique [14], as is shown in Figure 3.

Looking from the back of the wind tunnel the left vortex is larger and more persistent than the right vortex, and this is due to the combined effect of the wheel camber angle and strut. Figure 3 also shows details of the vortical structures

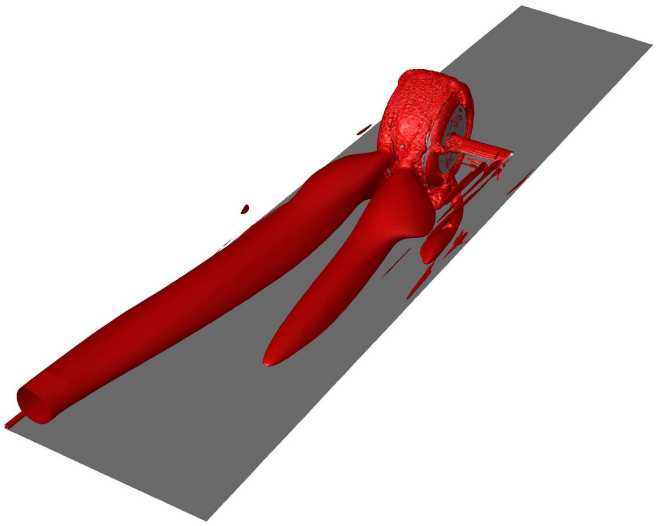

Figure 3: Isosurface of constant λ_2 showing vortical structures around and in the wake of the wheel

emanating from the front of the contact patch, following the path of the shear layer. The interaction of the strut with the wall of the wind tunnel also creates small vortical structures that advect with the main flow downstream.

VORTEX CORE LOCATIONS AT PLANE X/D=1.12 The computed flow field in the wake of the tire is very sensitive to the type of RANS closure chosen.

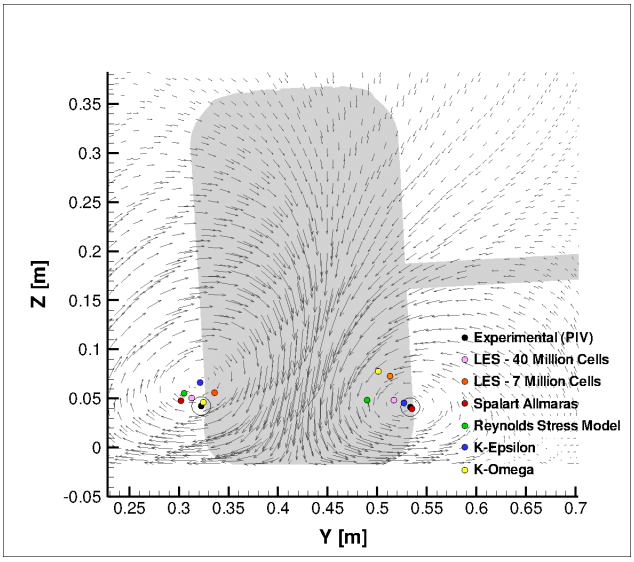

Figure 4: Comparison of vortex core locations using LES, PIV, and RANS data

Although qualitatively all the RANS models are similar,Figure 4 shows the variability of the two vortex core locations for the counter-rotating vortices at a plane x/D=1.12 downstream from the center of the tire. The in-plane velocity vectors are plotted for the k-ϵ model, hence the blue dots correspond to the vortex cores of the shown velocity vectors.

The black dot in the figure represents the experimental location of the vortex core based on the PIV vectors of inplane velocity. The black circle around the black dot quantifies the maximum margin of error for the experiment. Quantifying the maximum margin of error for the RANS models is challenging, and is a topic that will be covered in another study. All the RANS models as well as the coarse LES simulation use the exact same mesh.

If the instantaneous flow field is plotted for a plane in the wake of the LES simulation there are no apparent coherent structures on a macro scale. The flow-field looks similar to an instantaneous PIV image showing small eddies randomly distributed in the plane. If the flow for the fine LES simulation is averaged over all timesteps over an interval of 5 ms (approximately 1000 timesteps), the location of the vortex core becomes clear. If all these points are plotted versus time, we can investigate how these vortices oscillate in time.

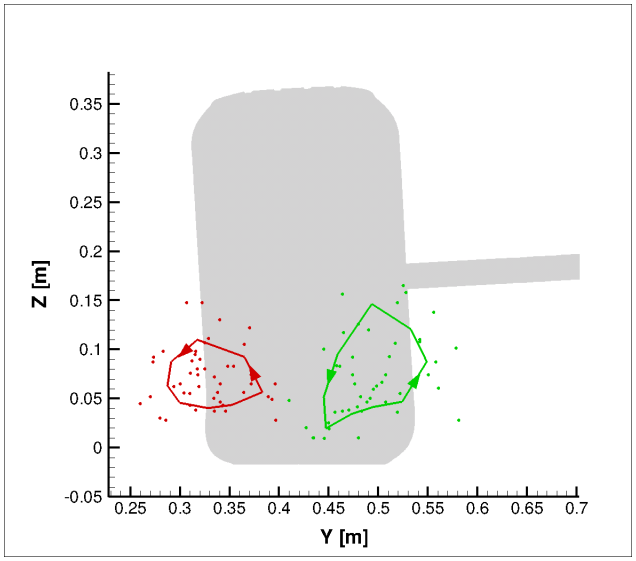

Figure 5: Instantaneous vortex core locations (dots) and phase-averaged trajectory of both the left and right vortex cores

Figure 5 shows the location of the instantaneous vortex cores plotted in the x/D=1.12 plane. A timescale for the turnover time of the vortex core location is determined by computing the angle ($\theta(t)$) of the vortex core location with respect to the mean vortex core location; one full revolution is defined as the vortex core turnover time. Defining the flow-through time as the diameter of the wheel divided by the freestream velocity, the vortex core turnover time is approximately twice the flow-through time. The averaged eddy turnover time (which is determined by computing the mean vortex radius and tangential velocity) is approximately equal to one flow-through time. The streamwise velocity in the near wake of the tire is much smaller than the freestream velocity, therefore a particle very close to the vortex core will undergo a minimum of 10 revolutions prior to reaching the plane located at x/D=1.

Figure 5 also shows a mean trajectory for both the left and right vortex cores. This was determined by computing the average distance between the vortex core and the mean vortex core location as a function of $\theta(t)$. With this information, the data can be sorted from 0 to 360 degrees and subdivided into 'n' bins such that there are enough samples to compute an average radius and angle for every bin. The results show that on average the left vortex core follows a clockwise circular path. While the right vortex has a more elongated counter-clockwise shape showing a positive correlation between the y and z coordinate. This essentially means that on the average the right vortex is moving either in a northeasterly or southwesterly fashion. The direction of rotation for the trajectory of both vortex cores matches the rotation of the time averaged flow.

VELOCITY PROFILES IN NEAR WAKE OF TIRE The fine grid LES contour plot of the inplane-velocity for the constant Y centerplane of the tire is shown Figure 6(a). The inplane-velocity ($\sqrt{u^2 + w^2}$) is defined as the square root of the sum of the square of the u and w velocities (i.e. velocities corresponding to the streamwise and vertical directions respectively). The five black lines in the wake of the tire correspond to the five locations that were chosen to compare streamwise and vertical velocity profiles (at x/D=[0.60,0.83,0.95,1.08,1.21]).

Figure 6(b) shows the sensitivity of the streamwise velocity profile to turbulent intensity, turbulence model, and camber angle. The difference between the 2.5° and 3.25° camber angle is not discernible in this plane due to the fact that this plane is furthest away from both the inboard and outboard edges (this plane is least affected by incorrect modeling of the tire shoulder). The camber effect should be amplified in planes near the inboard and outboard sides of the tire. Also inlet turbulent intensity does not have an effect on the velocity profiles below the shear layer, but there is a difference in streamwise velocity above the shear layer for different turbulent intensities.

Figure 6(c) shows a strong downwash region with the peak downwash velocity decreasing both in magnitude and in height from the ground plane as the flow is convected downstream. Quantitatively all RANS and LES simulations accurately predict the correct curvature of the experimental velocity profile, with the LES simulation matching closest to the PIV data.

Moving now to the outboard plane, Figure 7(a) shows a contour plot of inplane-velocity that is qualitatively different from the centerplane. The shear layer stays at a constant height from the ground, and there is no evidence of any strong downwash region as is shown in Figure 7(c). The LES profiles of Figure 7(c) have oscillations due to the insufficient time averaging of the solution. Regions of low velocity require much longer averaging time but are not expected to affect the statistics in other areas with much lower residence time. When comparing the streamwise velocity for this plane, the streamline curvature of the simulations compared to the experimental velocity

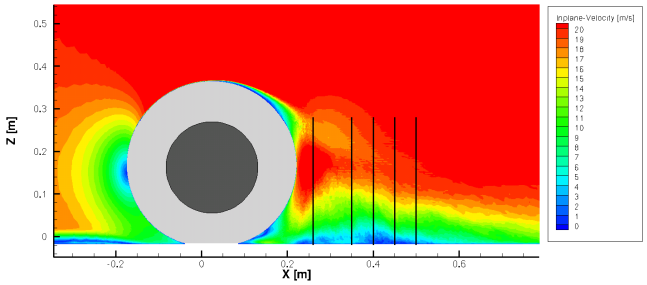

(a) Contour plot of inplane-velocity

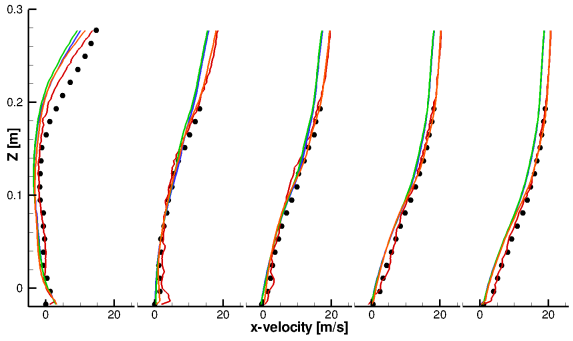

(b) Streamwise velocity comparison of LES, PIV, and RANS data

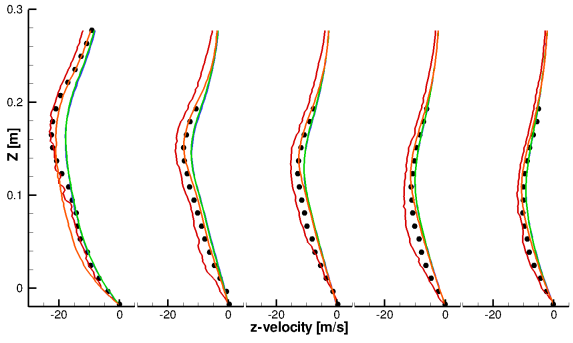

(c) Vertical velocity comparison of LES, PIV, and RANS data

Figure 6: Centerplane velocity comparison (Experiment - Black Dots, LES at 3.25° - Red, RANS at 3.25° with 5% TI - Blue, RANS at 3.25° with 1% TI - Orange, RANS at 2.5° with 5% TI - Green)

profiles is not consistent. The magnitude of streamwise velocity close to the ground is under predicted, but the velocity just above shear layer is over predicted. It is interesting to note that the inflection points for all profiles are comparable. This is an indication that the separation bubble is tilted differently in the simulations than what has been measured.

Finally, the inboard plane shown in Figure 8 captures the curvature of streamwise velocity correctly, but the magnitude of velocity is under predicted compared to the PIV profile. Once again, this plane shows very low levels of downwash velocity. The largest difference between the 3.25° camber and 2.5° is evidenced in Figure 8(c) which is to be expected because this is a plane very close to edge of the tire; small changes in camber angle affect this plane more than the centerplane.

Figure 9 shows the inplane-velocity (now defined as $\sqrt{v^2 + w^2}$) for a cross flow plane in the wake of the tire at a location x/D=1.12. At the inboard and centerplanes the difference between the lines of constant inplane velocity are small, while there is a large discrepancy near the top of the outboard velocity profile. This suggests that the experiment has a larger wake near the top of the tire which leads to the over prediction of streamwise velocity in the RANS and LES simulations. While at a height Z=0.1m, the wake is slightly larger in the simulations which results in an under prediction of streamwise velocity in 7(b). Since these discrepancies are insensitive to the type of turbulence model (LES vs. RANS), this appears to be the result of incorrectly modeling the geometry (tire side walls, strut, etc.).

CONTOUR PLOT OF VELOCITY AT REAR OF CONTACT PATCH A very detailed analysis of the region directly behind the contact patch was also carried out to compare how LES and RANS perform in a region that is dominated by separated flow, recirculation bubbles, and turbulence anisotropy. Figure 10 shows the selected region of interest for this study.

The PIV window and CFD window are not of the same size due to optical access limitations of the wind tunnel. Nine Y planes systematically chosen to coincide with the four treads of the tire are compared, but only the results of 3 planes (inboard, centerplane, and outboard) are shown. The reason for choosing planes intersecting the tire grooves was to determine if there was any flow passing through the four channels formed between the grooves and ground. The results of a preliminary study show that there is very little flow actually passing through the channels. The main difference between the computational CFD model and experimental model is that there are no grooves in the CFD model; this difference is shown to be insensitive to the coherent wake structures.

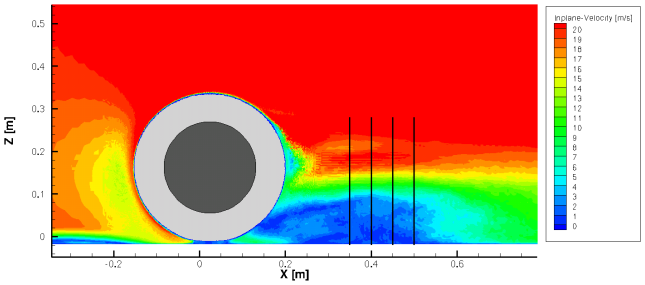

(a) Contour plot of inplane-velocity

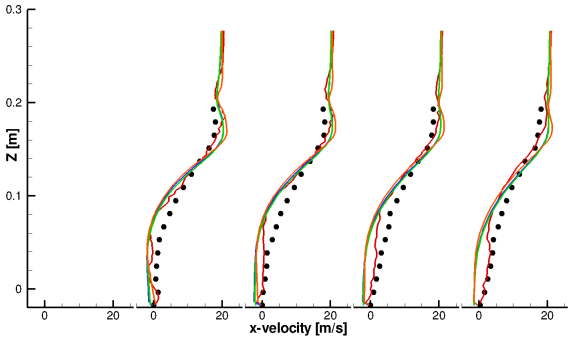

(b) Streamwise velocity comparison of LES, PIV, and RANS data

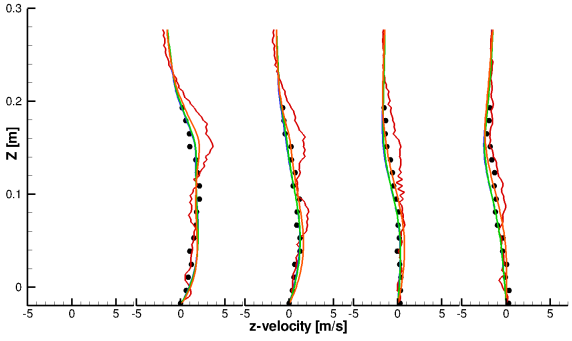

(c) Vertical velocity comparison of LES, PIV, and RANS data

Figure 7: Velocity comparison of a plane y/W=0.5 outboard from the centerplane (Experiment - Black Dots, LES at 3.25° - Red, RANS at 3.25° with 5% TI - Blue, RANS at 3.25° with 1% TI - Orange, RANS at 2.5° with 5% TI - Green)

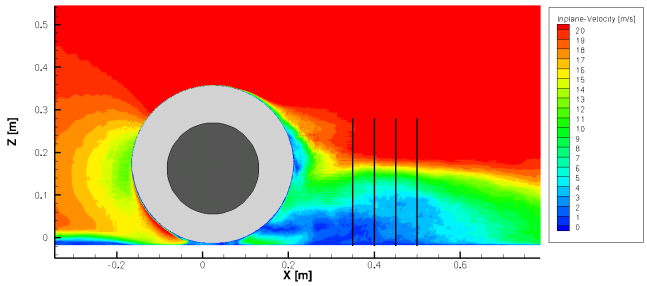

(a) Contour plot of inplane-velocity

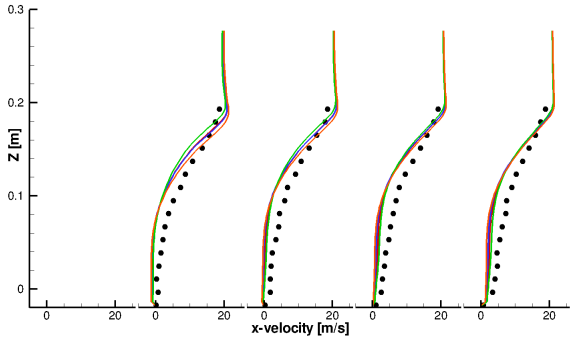

(b) Streamwise velocity comparison of LES, PIV, and RANS data

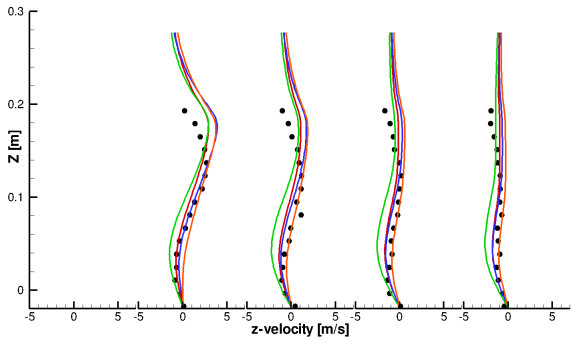

(c) Vertical velocity comparison of LES, PIV, and RANS data

Figure 8: Velocity comparison of a plane at y/W=-0.5 (measured from the centerplane of the tire and based on width [W] of tire) inboard from the centerplane (Experiment - Black Dots, LES at 3.25° - Red, RANS at 3.25° with 5% TI - Blue, RANS at 3.25° with 1% TI - Orange, RANS at 2.5° with 5% TI - Green)

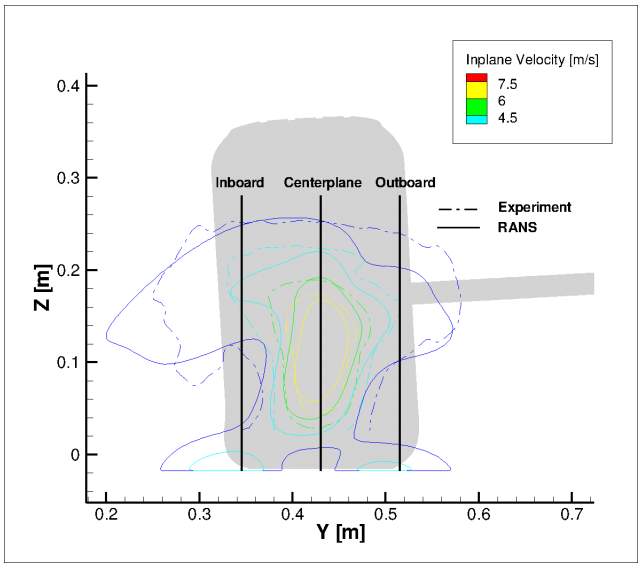

Figure 9: Comparison of PIV and RANS inplane-velocity in the wake of the tire at a plane x/D=1.12. The locations of the 3 streamwise planes (inboard, centerplane, outboard) are also shown.

Figure 11(a) shows the inplane-velocity for the inboard plane. By looking at the velocity vectors (Figure 12(a) for all three datasets they are all qualitatively similar in that the flow is completely reversed (no component of the inplane-velocity has a positive streamwise velocity). In general the flow is moving in a northwesterly direction which indicates the flow stagnates near the bottom of the contact patch at the centerplane, and splits towards each side of the tire. As the flow approaches the inboard side of the tire it moves upstream and upwards toward the center of the tire.

Comparing the centerplane velocities (Figure 11(b)) shows the PIV and LES flowfields are similar both in magnitude and in direction as is shown by the velocity vectors of Figure 12(b). They both capture the recirculation bubble just above the rear contact patch as well as the bifurcation in the flow (the flow stagnates). The RANS simulation is not able to capture neither the recirculation bubble or the bifurcation.

The velocity vectors of the outboard plane (Figure 12(c)) are qualitatively similar to the inboard plane in that all three datasets are comparable in terms of direction of the flow, but the magnitude of inplane velocity is higher for the outboard plane. RANS under predicts the inplane-velocity in this region almost by a factor of 2, while LES is more comparable to the PIV data.

The magnitude of inplane-velocity for the LES simulation matches with the centerplane, but it over predicts the

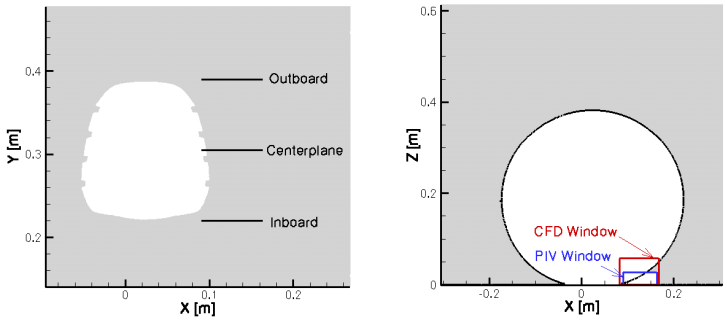

Figure 10: Description of locations of PIV and CFD windows. Left: Location of PIV Planes shown from above. Right: Comparison of the CFD and PIV windows viewing the tire from its side.

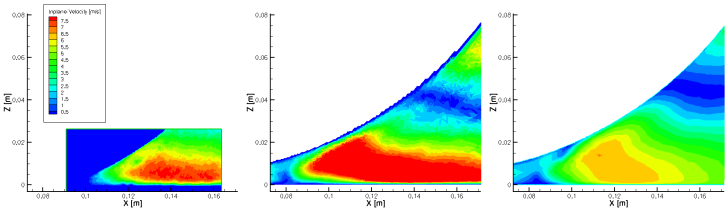

(a) Inboard Plane

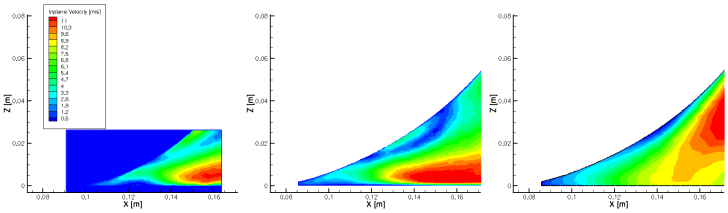

(b) Centerplane

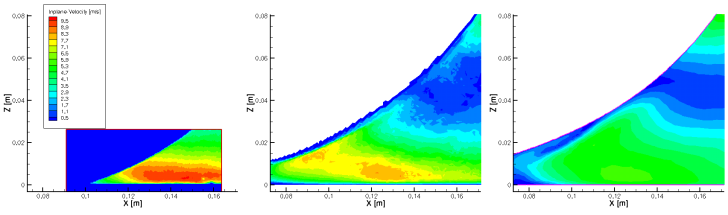

(c) Outboard Plane

Figure 11: Contour plot of inplane-velocity for three planes near the rear contact patch of the tire. Left: Experiment (2.5°), Center: Fine Mesh LES (3.25°), Right: RANS RKE (2.5°)

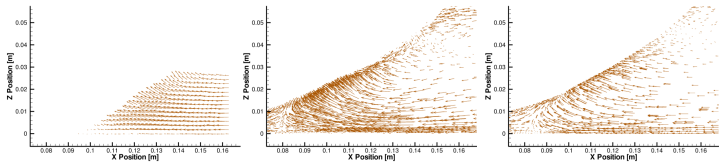

(a) Inboard Plane

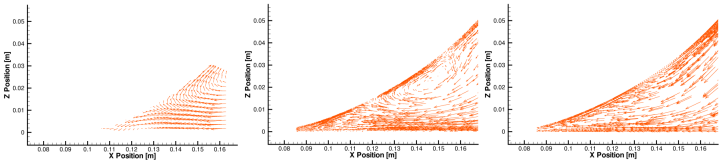

(b) Centerplane

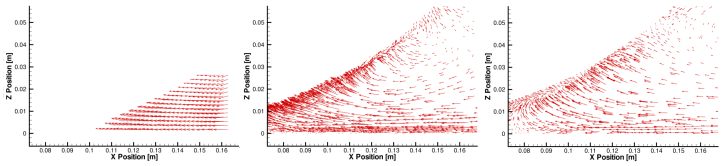

(c) Outboard Plane

Figure 12: Velocity vectors of inplane-velocity for three planes near the rear contact patch of the tire. Left: Experiment (2.5°), Center: Fine Mesh LES (3.25°), Right: RANS RKE (2.5°)

inplane-velocity for the inboard plane while under predicting the velocity for the outboard plane. This seems to suggest that the influence of camber angle is important (the PIV data is for 2.5°, while the LES simulation is for 3.25° camber angle), and does change the flow features in the vicinity of the contact patch. On the other hand, RANS simulations consistently under predict the inplane-velocity compared to the PIV data.

CONCLUSIONS

The wake dynamics of a 60% scale Formula 1 tire was investigated in order to compare the sensitivity of the wake to different turbulence closures. The sensitivity to turbulence model was shown by comparing the vortex core locations for RANS, PIV, and LES. Quantitatively, the locations of the vortex cores for the fine LES simulation match closest with the PIV vortex cores. Performing an LES simulation of the flow around a bluff body is more accurate than RANS in regions of highly separated flow, recirculation regions, as well as regions where the flow is three dimensionally non homogeneous. The difference between LES and RANS decreases as the flow moves downstream. This is evidenced by plotting streamwise velocity profiles for x/D $>$ 1. There is very good agreement with both LES and RANS when comparing the Y centerplane inplane-velocity with the PIV data even for x/D $<$ 1. This is due in part to the strong downwash region immediately behind the tire. Finally, the curvature and magnitude of the PIV streamwise velocity for both the inboard and outboard planes does not match well with the RANS and LES data; a reason for the discreptancy could be due to incorrect modeling of the deformable tire shoulder and contact patch. To conclude, if time constraints permit, an LES simulation is perferred over a RANS simulation if a more accurate description of the flowfield is required; this is based on comparing both datasets to the available PIV data.

ACKNOWLEDGMENTS

The authors wish to thank Toyota Motor Corporation - F1 Motorsports Division for their financial support of this work, as well as Dr. Frank Ham for providing technical expertise and the code used for the LES simulations in this paper.

REFERENCES

[1] Wright P. (2004), Ferrari Formula 1: Under the Skin of the Championship Winning F1-2000, ISBN 978-0-7680-1341-2, Warrendale, PA

[2] Spalart P. R. (2000) Strategies for turbulence modelling and simulations, International Journal of Heat and Fluid Flow, Vol 21, Issue 3, pp 252-263

[3] Fackrell J. E., Harvey, J. K. (1973), The Flow Field and Pressure Distribution of an Isolated Road Wheel, Advances in Road Vehicle Aerodynamics, Paper 10, pp. 155-165, BHRA.

[4] Nigbur J. E. (1999), Characteristics of the wake downstream of an isolated automotive wheel, MSc Thesis, Cranfield University, Bedfordshire, UK

[5] Wäschle A., Cyr S., Kuthada T., Wiedermann J. (2004), Flow around an isolated wheel - experimental and numerical comparison of two CFD codes, Technical Paper 2004-01-0445, Society of Automotive Engineers

[6] McManus J., Zhang X. (2006), A Computational Study of the Flow Around an Isolated Wheel in Contact With the Ground, ASME J. Fluids Eng., **128**, pp. 520-530

[7] Knowles R. D., Saddington A. J., Knowles K. (2002), On the Near Wake of Rotating, 40%-Scale Champ Car Wheels, Technical Paper 2002-01-3293, Societey of Automotive Engineers

[8] Saddington A. J., Knowles R. D., Knowles K. (2007), Laser Doppler anemometry measurements in the near-wake of an isolated Formula One wheel, Exp Fluids, DOI 10.1007/s00348-007-0273-7

[9] Fackrell J. E. (1972) The Aerodynamic Characteristics of an Isolated Wheel Rotating in Contact with the Ground, Ph.D. thesis, Imperial College, London, UK

[10] Ham F., Iaccarino G. (2004) Energy conservation in collocated discretization schemes on unstructured meshes, Center for Turbulence Research, Annual Research Briefs, Stanford, CA

[11] Shih T.H., Liou W.W., Shabbir A., Yang Z., Zhu J., (1995), A New k-ϵ Eddy Viscosity Model for High Reynolds Number Turbulent Flows, Comput. Fluids, **24**(3), pp. 227-238

[12] Basara B., Beader D., Przulj V. (2000), Numerical Simulation of the Air Flow Around a Rotating Wheel, 3rd MIRA International Vehicle Aerodynamics Conference

[13] Axon L. (1999), The Aerodynamic Characteristics of Automobile Wheels - CFD Prediction and Wind Tunnel Experiment, Ph.D. thesis, Cranfield University, Bedfordshire, UK

[14] Barbone L., Gattei L., Rossi R. (2005) Identification and analysis of turbulent structures around a simplified car body, Proceedings of the 2nd European Automotive CFD Conference, Frankfurt, Germany